

# Low Power Battery Supervisory Circuit with Adaptive Battery Health Monitor

Inhee Lee, Yoonmyung Lee, Dennis Sylvester, David Blaauw  
University of Michigan, Ann Arbor, MI

## Abstract

We propose a battery supervisory circuit (BSC) for wireless sensor nodes that automatically adapts to varying battery health, as reflected by its internal resistance ( $R_{BAT}$ ), and establishes a constant effective threshold voltage. Compared to a conventional fixed-threshold BSC, the new design avoids oscillation and widens the usable range of battery voltages, independent of  $R_{BAT}$ .  $R_{BAT}$  is measured by inducing a test current using decaps and measuring the resulting battery RC response time. When tested with a  $2\mu\text{Ah}$  battery and  $11\mu\text{A}$  sensor system, the BSC reduces the required hysteresis from  $656\text{mV}$  to  $77\text{mV}$ , increasing the usable battery voltage range by  $2.7\times$ .

## Introduction & Conventional BSCs

Rapid advances in low-power wireless sensor nodes are driving the realization of Internet of Things [1]. Wireless sensor nodes often include an energy harvester that takes energy from a source (e.g., solar cell) and transfers it to a battery (Fig. 1). Battery voltage ( $V_{BAT}$ ) varies over time depending on the amount of harvested energy vs. system energy consumption. To avoid unpredictable circuit behavior, a battery supervisory circuit (BSC) monitors  $V_{BAT}$  and only enables the system when  $V_{BAT}$  exceeds a certain threshold. Conventional BSCs [2-4] typically include a  $V_{BAT}$  divider, voltage reference, comparator, and delay generator (Fig.1, bottom). The divided  $V_{BAT}$  ( $V_{DIV}$ ) is compared to a predetermined threshold voltage ( $V_{TH}$ ) (generated using a voltage reference) by a comparator. The output (*compout*) either immediately disables the sensor system or enables it after a delay that provides stabilization time to the circuits.

To prevent oscillation, conventional BSCs employ two fixed threshold voltages, controlled by an enable signal (Fig. 1). The lower threshold voltage,  $V_{DISABLE}$ , sets the lowest  $V_{BAT}$  voltage at which circuits operate properly. The higher threshold voltage,  $V_{ENABLE}$ , provides hysteresis ( $V_{HYST} = V_{ENABLE} - V_{DISABLE}$ ) to prevent the system from oscillating between enabled and disabled modes.

In a battery-operated system, the required  $V_{HYST}$  value is directly related to the battery internal resistance ( $R_{BAT}$ ). When  $V_{BAT}$  first reaches  $V_{ENABLE}$  and the sensor node turns on, the additional current draw from the system ( $I_{SYSTEM}$ ) causes an immediate  $I_{SYSTEM}\times R_{BAT}$  battery voltage drop. Conversely, when the system is disabled, the reduced  $I_{SYSTEM}$  creates an upward spike in  $V_{BAT}$ . If these IR spikes exceed  $V_{HYST}$ , the system will oscillate (Fig. 2).

Miniature wireless sensor nodes are unique in that they employ very small batteries with high  $R_{BAT}$ , e.g.,  $7\text{k}\Omega$  [5], leading to large IR drops. Battery health declines with discharge cycles, increasing  $R_{BAT}$  (e.g., from  $7 - 31\text{k}\Omega$  over 1000 cycles [5]) and is also temperature dependent [6]. As a result, the current BSC approach requires a large  $V_{HYST}$  to accommodate the worst-case  $R_{BAT}$  over its lifetime, which both delays system turn-on time and reduces the usable range of battery voltages ( $V_{USE}$ ) over which the system can operate.

## Proposed BSC

We propose a new BSC that dynamically modifies  $V_{ENABLE}$  (and hence  $V_{HYST}$ ) to adapt to the varying  $R_{BAT}$ , obtaining an  $V_{ENABLE,EFF}$  that is constant and independent of  $R_{BAT}$  (Fig. 3). When  $V_{BAT}$  reaches  $V_{ENABLE}$ , the  $R_{BAT}$  monitor first measures  $R_{BAT}$  by inducing a test current using decoupling capacitors and measuring the RC response.  $V_{ENABLE}$  is then updated to ' $V_{ENABLE,EFF} + R_{BAT} \times I_{SYSTEM,MAX}$ ' using a low-power divided voltage reference.  $V_{BAT}$  is compared against the new  $V_{ENABLE}$  and enabled if  $V_{BAT} > V_{ENABLE}$ . Otherwise, the system waits for  $V_{BAT}$  to increase until  $V_{BAT} > V_{ENABLE}$ , at which point the process repeats. This approach ensures that  $V_{BAT}$  remains higher than  $V_{ENABLE,EFF}$  after the system is enabled. The technique requires knowledge of  $I_{SYSTEM,MAX}$ , which is feasible in small wireless systems that typically have well-defined operation. In the proposed approach, the effective  $V_{HYST} = V_{ENABLE,EFF} - V_{DISABLE}$  and is independent of  $R_{BAT}$ . Hence,  $V_{HYST}$  does not need to be margined for changes in  $R_{BAT}$ ,

maximizing the useable voltage range over system lifetime.

Fig. 4 shows the proposed BSC circuit diagram. The  $V_{BAT}$  divider uses 65 diode-connected PMOS transistors that give a division ratio of 3.25/3.05 when *enable* = 0/1. The  $V_{TH}$  generator includes a leakage-based voltage reference/divider and provides 64 possible analog reference voltages from 1.06V to 1.28V for the adaptive  $V_{TH}$ . This reference consumes 77pA (simulated) while providing 319ppm/ $^{\circ}\text{C}$  TC and 0.17%/V line sensitivity (measured). It is constructed with a zero- $V_{TH}$  NMOS transistor for leakage generation at the top of a stack and diode-connected PMOS transistors that provide multiple outputs. When  $V_{DIV} > V_{TH}$ , the  $R_{BAT}$  monitor is triggered and produces *dout* (6-bit code), which updates the  $V_{TH}$  generator based on the current  $R_{BAT}$  value. If this causes  $V_{DIV} < V_{TH}$ , *enable trigger* will remain low since  $R_{BAT}$  detection (17.8ms) is much faster than the power-on-reset (PoR) delay ( $>50\text{ms}$ ).

Fig. 5 shows the proposed  $R_{BAT}$  monitor including the test current generator and RC response calculator. The test current generator operates by first placing decoupling capacitors in series to discharge them (Steps 1 – 3). This is done gradually to avoid  $V_{BAT}$  overshoot, which can damage circuits in the system. In the final step (4) all capacitors are placed in parallel simultaneously, creating a large current draw from the battery. This results in an RC voltage curve on  $V_{BAT}$  with a time constant of  $R_{BAT}\times(\Sigma C_{DC,i})$ . This time constant is measured by comparing  $V_{DC}$  with its earlier sampled and divided version  $V_{SAMP}$ . A fast ripple counter quantifies the time when  $V_{DC} < V_{SAMP}$ . Since  $V_{SAMP}$  is relative to  $V_{BAT}$ , *dout* is insensitive to the system.

Note that switch  $S_1$  is open during Step 4, protecting the system from the test-induced voltage drop. Since the system operates from a decoupling capacitance during this time, the test event is kept short ( $<65\mu\text{s}$ , measured). Note that the test capacitors ( $C_{DC1}-C_{DC4}$ ) act as standard decoupling capacitors in normal operation. The test chip implementation uses 8 test capacitors to limit  $V_{BAT}$  overshoot to 5.6% of  $V_{BAT}$  (measured). Fig. 6 describes clock generation, which includes a slow clock generator for Steps 1 – 3 and a fast clock generator for counting *dout*. The fast clock generator runs off a supply regulator that isolates it from the test-induced voltage drop on  $V_{BAT}$ .

The delay generator (Fig. 4) uses a voltage reference ( $V_{REF1}$ ) to drive a current source ( $I_{DELAY} = 3.3\text{nA}$ ). This charges a capacitor ( $C_{DELAY}$ ) that is compared to a second (configurable) voltage reference ( $V_{REF2}$ ) to set the PoR delay. Reference  $V_{REF1}$  compensates the TC of the resistor, resulting in a temperature insensitive delay (0.9%/ $^{\circ}\text{C}$  TC, 9.7%/V line sensitivity, measured).

## Measurement Results

Fabricated in 180 nm CMOS, the BSC was tested with a miniature  $2\mu\text{Ah}$  thin-film battery ( $1.375\times 0.85\text{mm}^2$ ) and a sensor system with  $I_{SYSTEM,MAX} = 11\mu\text{A}$ . The BSC draws 1nA during battery monitoring and 10nJ/conv. for  $R_{BAT}$  detection. Fig. 7 shows measured  $V_{TH}$  waveforms as it adjusts to  $R_{BAT}$  detection. Fig. 8 shows measured *dout* and  $V_{ENABLE}$ , demonstrating good matching across battery resistance. Fig. 9 shows a 500 cycle test of the BSC with the  $2\mu\text{Ah}$  battery, showing measured change in  $R_{BAT}$  from  $16\text{k}\Omega - 54\text{k}\Omega$ . The BSC has a maximum  $V_{HYST}$  tracking error of 27mV. Assuming 50mV margin, the proposed system requires an effective  $V_{HYST} = 50+27 = 77\text{mV}$ . In comparison a conventional BSC requires 656mV hysteresis to accommodate the worst-case  $R_{BAT} = 54\text{k}\Omega$  condition after 500 cycles. The proposed BSC therefore provides  $2.7\times$  usable battery voltage range ( $V_{BAT} \text{ min/max} = 3.2\text{V}/4.2\text{V}$ ). Fig. 10 shows standby-mode power and PoR delay. Figs. 11 and 12 show the die photo and a performance summary with comparison table.

## References

- [1] K. Ashton, *RFID J.*, 2009.
- [2] H. Le *et al.*, TCAS2, 2011.
- [3] I. Lee *et al.*, VLSI, 2012.
- [4] TPS3839, Texas Instruments.
- [5] CBC005, CYMBET.
- [6] H.J. Bergveld *et al.*, Battery Management Systems. 2002.

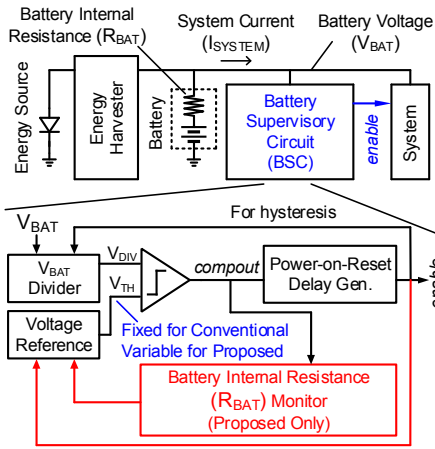


Figure 1. Battery supervisory circuit (BSC) for a wireless sensor node. (Red: Proposed only)

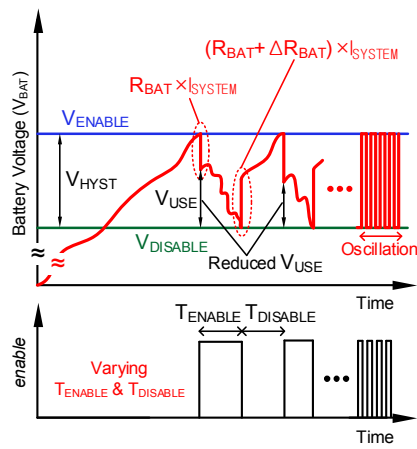


Figure 2. Operation of conventional BSC with fixed-threshold voltages.

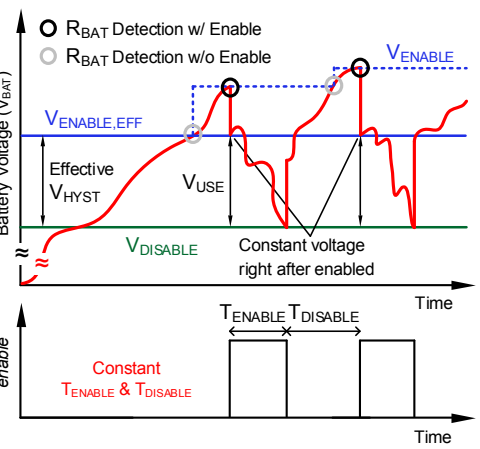


Figure 3. Operation of proposed BSC with adaptive-threshold voltage ( $V_{ENABLE}$ ).

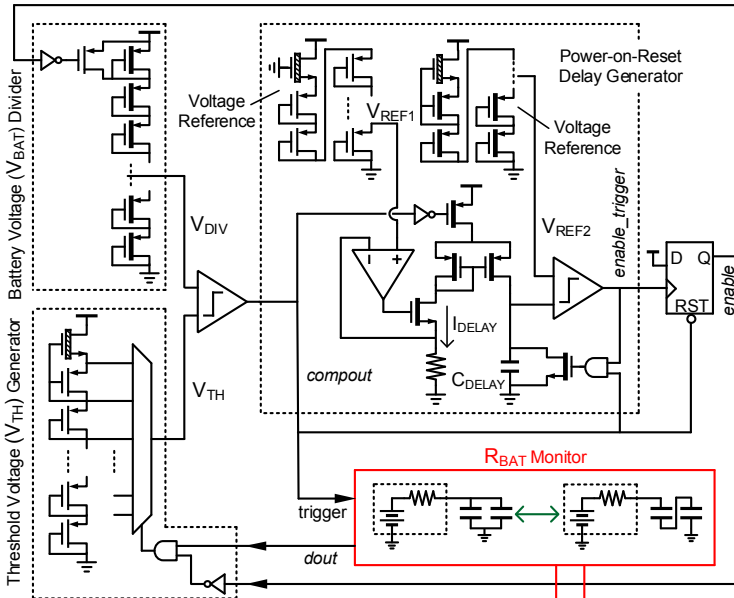


Figure 4. Circuit diagram of proposed BSC with  $R_{BAT}$  monitor.

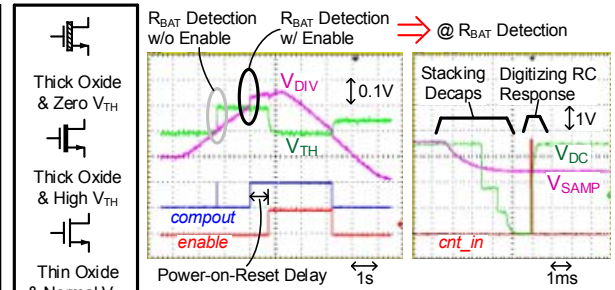


Figure 7. Measured oscilloscope waveforms.

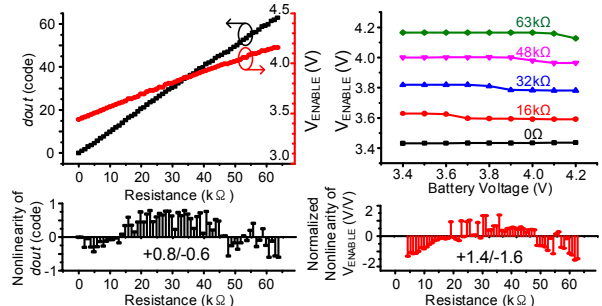


Figure 8. Measured  $dout$  &  $V_{ENABLE}$  over  $R_{BAT}$  &  $V_{BAT}$ .

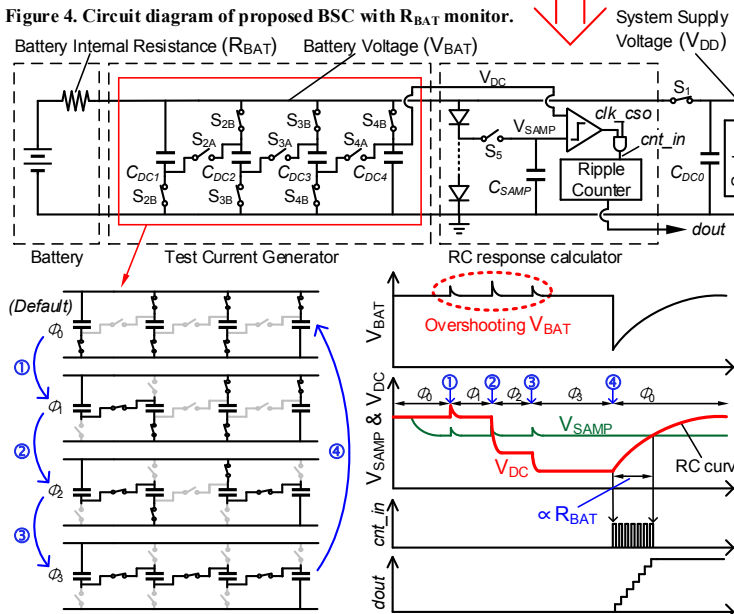


Figure 5. Circuit diagram and operation of proposed  $R_{BAT}$  monitor.

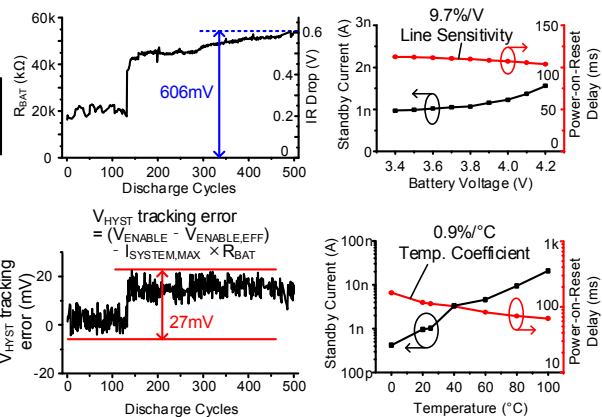


Figure 9. Measured  $R_{BAT}$  over discharge cycles &  $V_{HYST}$  tracking error.

Figure 10. Measured standby power & power-on-reset delay.

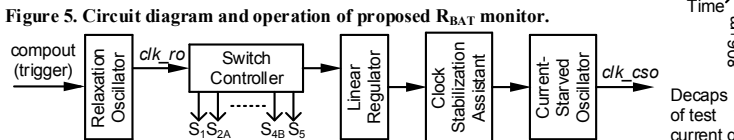


Figure 6. Clock and control signal generation for  $R_{BAT}$  monitor.

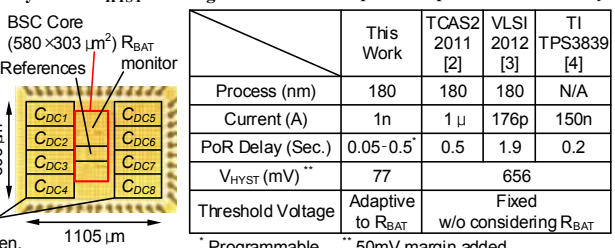


Figure 11. Die Photo.

	This Work	TCAS2 2011 [2]	VLSI 2012 [3]	T1 TPS3839 [4]
Process (nm)	180	180	180	N/A
Current (A)	1n	1 μ	176p	150n
PoR Delay (Sec.)	0.05-0.5	0.5	1.9	0.2
$V_{HYST}$ (mV)	77	656		
Threshold Voltage	Adaptive to $R_{BAT}$	Fixed w/o considering $R_{BAT}$		

Figure 12. Performance Summary & Comparison.